

Citation for published version:

Rong, Y, Malpass-Evans, R, Carta, M, McKeown, NB, Attard, GA & Marken, F 2014, 'Intrinsically porous polymer protects catalytic gold particles for enzymeless glucose oxidation', *Electroanalysis*, vol. 26, no. 5, pp. 904 - 909. <https://doi.org/10.1002/elan.201400085>

DOI:

[10.1002/elan.201400085](https://doi.org/10.1002/elan.201400085)

Publication date:

2014

Document Version

Peer reviewed version

[Link to publication](#)

University of Bath

Alternative formats

If you require this document in an alternative format, please contact:
openaccess@bath.ac.uk

General rights

Copyright and moral rights for the publications made accessible in the public portal are retained by the authors and/or other copyright owners and it is a condition of accessing publications that users recognise and abide by the legal requirements associated with these rights.

Take down policy

If you believe that this document breaches copyright please contact us providing details, and we will remove access to the work immediately and investigate your claim.

Revision

8th March 2014

Intrinsically Porous Polymer Protects Catalytic Gold Particles for Enzymeless Glucose Oxidation

Yuanyang Rong ¹, Richard Malpass-Evans ², Mariolino Carta ³, Neil B. McKeown ³,
Gary A. Attard ², and Frank Marken ^{*1}

¹ *Department of Chemistry, University of Bath, Claverton Down, Bath BA2 7AY, UK*

² *School of Chemistry, Cardiff University, Cardiff CF10 3AT, UK*

³ *School of Chemistry, University of Edinburgh, West Mains Road, Edinburgh,
EH9 3JJ, UK*

To be submitted to Electroanalysis

Proofs to F. Marken (f.marken@bath.ac.uk)

Abstract

The enzymeless glucose oxidation process readily occurs on nano-gold electrocatalyst at pH 7, but it is highly susceptible to poisoning (competitive binding), for example from protein or chloride. It is shown here that gold nanoparticle catalyst can be protected against poisoning by a polymer of intrinsic microporosity (PIM-EA-TB with BET surface area $1027 \text{ m}^2\text{g}^{-1}$). This PIM material when protonated, achieves a triple catalyst protection effect by (i) size selective repulsion of larger protein molecules (albumins) and (ii) membrane ion selection effects, and (iii) membrane ion activity effects. PIM materials allow “environmental control” to be introduced in electrocatalytic processes.

Keywords: glucose, fuel cell, sensor, microporosity, membrane, electrocatalysis.

1. Introduction

New materials in electrochemistry offer opportunities for improved devices and processes and in the recent years several cases of interesting novel porous solids, e.g. metal-organic frameworks [1], zeolitic materials [2], or mesoporous films [3], have emerged. In terms of polymeric materials, there have been many areas of progress including gels [4], conducting polymers [5], and brushes [6]. The recent development of polymers with intrinsic microporosity (PIMs) and similar novel materials [7] is particularly interesting with a range of potential applications in electrochemical technology. Uncharged PIM materials have been proposed [8] and developed for gas storage [9,10] gas separation [11,12,13], and as sensor component [14]. The structurally highly rigid and disordered PIM backbone achieves open packing to generate novel properties due to permanent microporosity. When charged, these PIM materials introduce ion selectivity, permselectivity, and further porosity effects which are closely linked to the molecular structure and functionalization of the backbone. Physicochemical characteristics are related to those observed for hydrogels [15,16] rather than those associated with polymeric systems. To date, potential applications are based on PIM-gas interaction, but our recent publication [17] has demonstrated benefits of PIM-electrolyte interactions and potential applications in solution phase electrocatalysis.

The preparation of amine-containing PIMs based on a polymerisation reaction involving the formation of Tröger's base (TB) was reported [18]. Thus, 2,6(7)-diamino-9,10-

dimethylethanoanthracene was polymerised with dimethoxymethane in trifluoroacetic acid to give PIM-EA-TB (Figure 1) with high molecular mass ($M_w > 70,000 \text{ g mol}^{-1}$) and with an apparent BET surface area of $1027 \text{ m}^2\text{g}^{-1}$. This polymer backbone is readily protonated at the tertiary nitrogens to give a rigid poly-cationic framework.

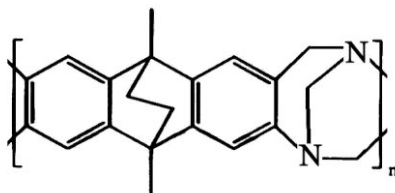


Figure 1. Molecular structure of PIM-EA-TB [18].

Glucose oxidation is studied predominantly in the context of glucose sensing, enzymatic [19] or non-enzymatic [20], and as *in vivo* energy source in enzymatic fuel cells [21]. The enzymeless oxidation of glucose on gold is of considerable interest [22,23] and can be seen as a more robust but less selective alternative technology. Pulse methods have been developed to overcome gold catalyst poisoning and interferences [24] and to control pH [25]. Chiral selectivity has been induced on gold electrocatalyst surfaces [26]. Novel high surface area gold electrodes have been proposed for more effective glucose oxidation even at lower pH [27,28] approaching conditions in blood serum. However, more progress is required to make gold nanoparticle catalysts as effective as biological catalysts. A considerable challenge remains in overcoming poisoning of the gold electrocatalysts under *in vivo* conditions.

It is shown here that the properties of PIM polymer membranes spin-coated over the gold nanoparticle catalyst can help protecting the catalyst from poisoning. The effect of the PIM membrane is studied (i) on the gold nanoparticle catalyst formation, (ii) on the electrocatalytic glucose oxidation mechanism, (iii) on the effect of protein on gold catalyst poisoning, and (iv) on the effect of chloride on gold catalyst poisoning in phosphate buffer at pH 7. PIM membranes are proposed as a versatile new class of materials for electrochemistry in particular for controlling the reaction environment in electrocatalytic processes.

2. Experimental

2.1. Chemical Reagents

Potassium gold(III) tetrachloride, D-(+)-glucose, albumin from bovine serum, sodium chloride, phosphoric acid (85%), potassium chloride, sulphuric acid (95%-98%), and sodium hydroxide were purchased from Aldrich or Fisher Scientific and used without further purification. PIM-EA-TB was prepared following a literature recipe [18]. Solutions were prepared with filtered and deionized water of resistivity 18.2 M Ω cm from a Thermo Scientific water purification system (ELGA).

2.2. Instrumentation

A potentiostat system (IVIUM Compactstat) was employed with a Pt wire counter electrode and a KCl-saturated calomel reference (SCE, Radiometer, Copenhagen). The working electrode was prepared from ITO coated glass (tin-doped indium oxide films sputter-coated onto glass, active area 10 mm \times 10 mm, resistivity *ca.* 15 Ω per square)

obtained from Image Optics Components Ltd (Basildon, Essex, UK). ITO electrodes were rinsed with ethanol and water, heat-treated in a tube furnace (Elite Thermal System Ltd) for 30 minutes at 500 °C, and then re-equilibrated to ambient conditions. All experiments were conducted at a temperature of 293 ± 2 K.

2.3. Gold Nanoparticle Deposition Method

A gold(III) solution was prepared by dissolving 1 mM KAuCl_4 in 0.1 M KCl addition of sulphuric acid to pH 2. Electrodeposition was performed in chronoamperometry mode. ITO electrodes were pre-treated at 1 V vs. SCE for 10 s followed by plating at -0.2 V vs. SCE for 200 s, rinsing with water, and drying under ambient conditions.

2.4. Polymer with Intrinsic Microporosity Coating Method

Initially, a solution of 1 mg cm^{-3} PIM-EA-TB in chloroform was applied directly by dipping the electrode followed by drying under ambient conditions. Improved coatings were obtained by spin-coating (Laurell WS-650Mz-23NPP, 1500 rpm for 30 seconds).

3. Results and Discussion

3.1. Electrodeposition of Catalytic Gold Nanoparticles onto Tin-Doped Indium Oxide (ITO) Substrates

The gold electrodeposition approach was selected based on an aqueous solution of 1 mM KAuCl_4 in 0.1 M KCl at pH 2 (acidified with H_2SO_4). The deposition experiments were conducted at -0.2 V vs. SCE for 200 s (if not stated otherwise) to form a uniform deposit of gold nanoparticles on the ITO substrate (see Figure 2A,B). Particles are typically 100 nm to 200 nm in diameter and well distributed over the electrode surface.

In cyclic voltammetry experiments these gold deposits immersed in 0.1 M phosphate buffer at pH 7 give stable voltammetric responses (see Figure 3A) with gold oxidation (see peak I_{ox} at 0.80 V vs. SCE) and gold back-reduction (see peak I_{red} at 0.55 V vs. SCE) indicative of an active gold surface.

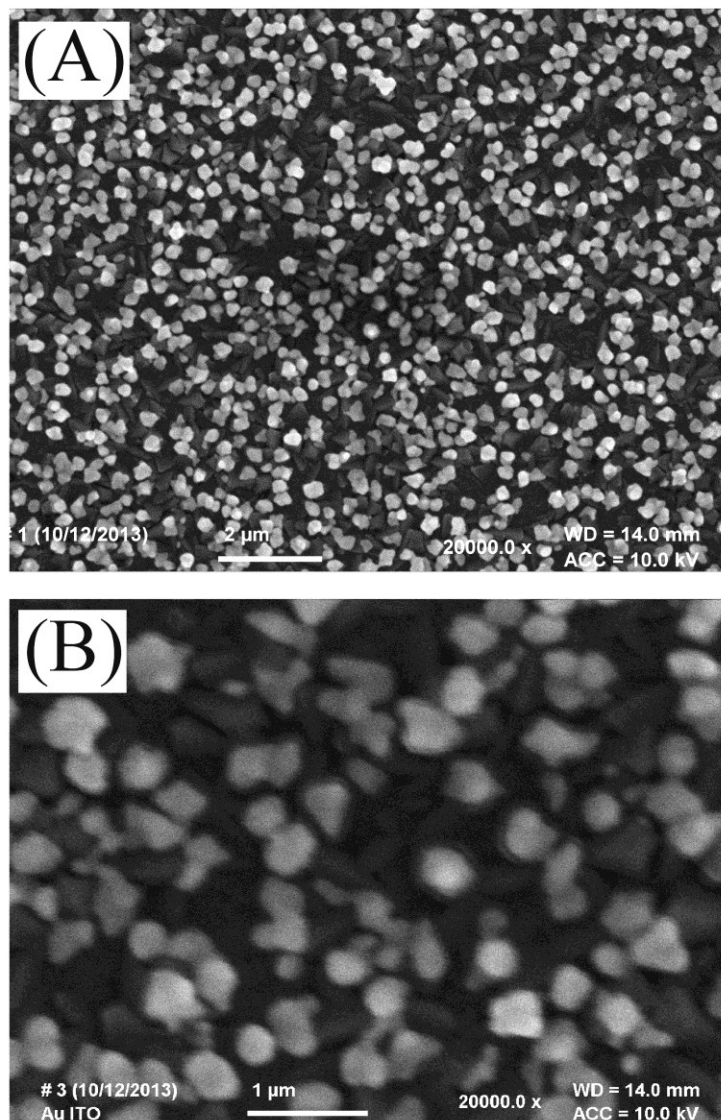


Figure 2. Scanning electron microscopy images for (A) gold nanoparticles grown on ITO for 200 s, (B) higher magnification image of gold nanoparticles.

The gold electrodeposition was repeated in the presence of a PIM film spin-coated onto the ITO surface (ca. 500 nm thickness). The same type of gold nanoparticle deposit was formed (confirmed by voltammetry and electrocatalysis experiments, *vide infra*). But unfortunately these films were unstable and easily peeled off the surface together with the

PIM film. Better quality films were obtained by first electroplating gold nanoparticles onto ITO and then coating with PIM. Drop-coating PIM resulted in film imperfection, but spin-coating a solution 1 mg cm^{-3} PIM in chloroform at 1500 rpm (see experimental) resulted in high quality film coatings.

3.2. Glucose Oxidation on Catalytic Gold Nanoparticles on Tin-Doped Indium Oxide (ITO) Substrates

The oxidation of glucose on gold nanoparticles immersed in phosphate buffer pH 7 has been reported previously and a typical anodic current peak is seen at 0.3 V vs. SCE (see Figure 3). As expected for a surface-catalytic kinetically controlled current response, this peak is not affected by scan rate (see Figure 3B) but strongly affected by the gold nanoparticle catalyst deposition time (see Figure 3C, peak II, note that this peak is observed most clearly during the potential sweep towards negative potentials). A plot of the effect of the gold nanoparticle deposition time on the glucose oxidation peak current is shown in Figure 3D. An improvement in the catalytic signal is seen up to approximately 400 s electrodeposition.

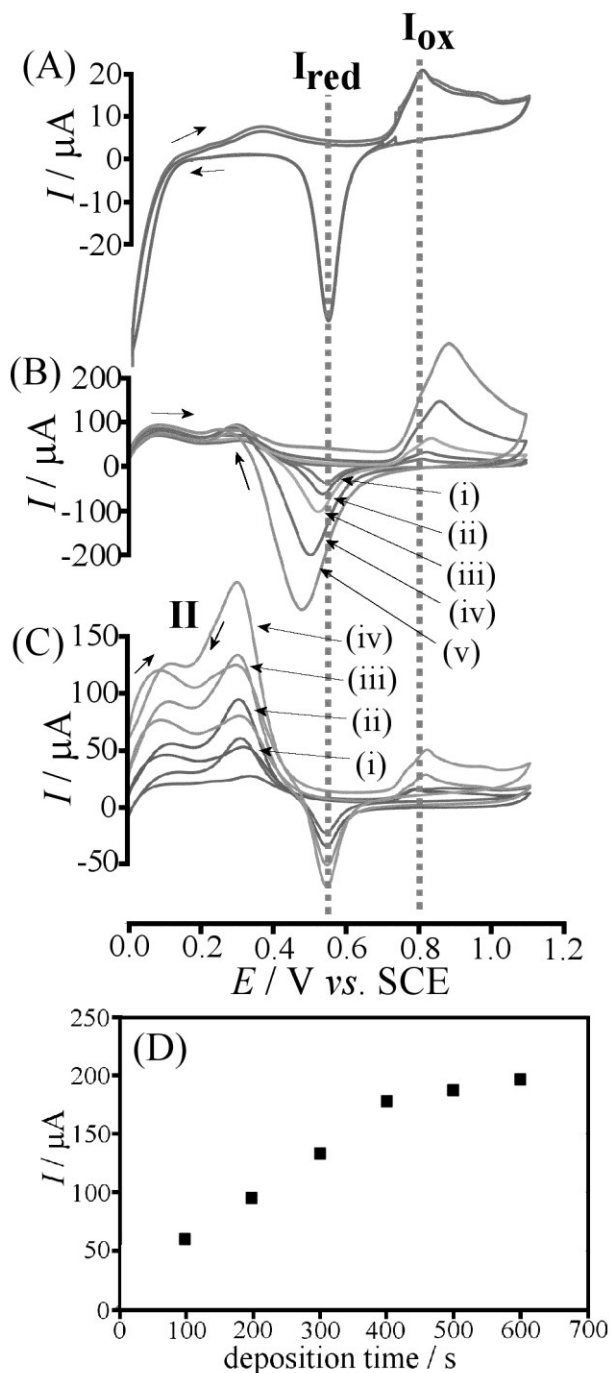


Figure 3. (A) Cyclic voltammograms (first and second cycle, scan rate 5 mVs^{-1} , start point 0.0 V vs. SCE) for gold nanoparticles on ITO immersed in 0.1 M phosphate buffer pH 7. (B) As before, but with 8 mM glucose and scan rate (i) 5, (ii) 10, (iii) 20, (iv) 50, (v) 100 mVs^{-1} . (C) As before, but with 8 mM glucose, scan rate 5 mVs^{-1} , and (i) 100 s, (ii) 200 s, (iii) 300 s, (iv) 600 s gold nanoparticle deposition time. (D) Plot of the glucose oxidation peak versus gold nanoparticle deposition time.

An investigation of the effect of the phosphate buffer concentration on the catalytic process provides further insight into the mechanism. As shown in Figure 4A a significant enhancement of the catalytic current for glucose oxidation is observed upon lowering the phosphate concentration. When plotted versus logarithm of phosphate concentration, the catalytic current exhibits an approximately linear dependence. This can be reconciled with a Langmuirian binding model where the kinetically controlled glucose oxidation current I_G is proportional to the coverage with glucose Θ_G at the active surface sites (equation 1).

$$I_G = \text{constant} \times \Theta_G = \text{constant} \times \frac{K_G[G]}{1 + K_G[G] + K_P[P]} \quad (1)$$

Here, K_G and K_P represent Langmuirian binding constants for glucose and a competing molecule or ion. For the special case of half coverage, that is $K_G[G] \approx K_P[P]$ (here observed for 8 mM glucose and 100 mM phosphate buffer), an approximately linear relationship around the point of half-coverage is possible, which suggests that here

$K_G/K_P \approx [P]/[G] \approx 12$. Therefore glucose is bound approximately an order of magnitude more strongly compared to other components in the phosphate buffer.

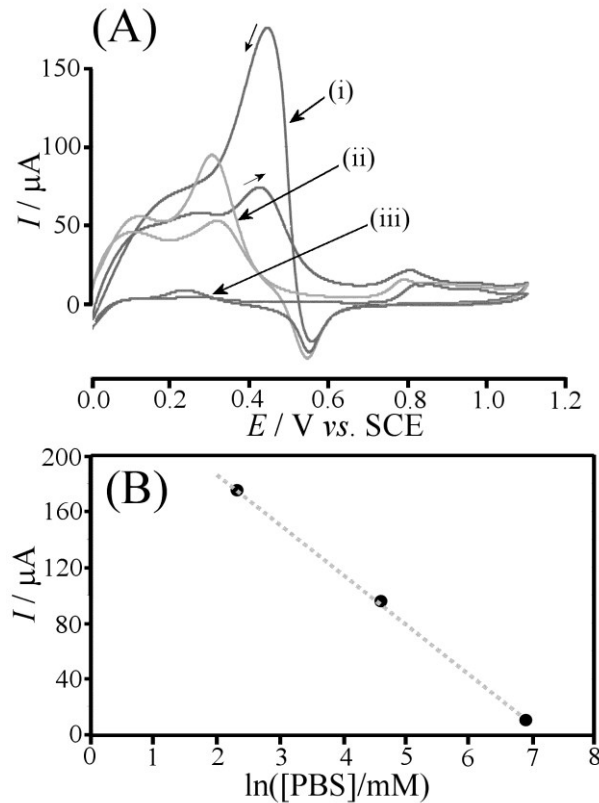


Figure 4. (A) Cyclic voltammograms (scan rate 5 mVs^{-1} , start point 0.0 V vs. SCE) for the oxidation of 8 mM glucose at gold nanoparticles on ITO immersed in (i) 10 , (ii) 100 , (iii) 1000 mM phosphate buffer pH 7 . (B) Plot of the peak current versus logarithm of phosphate buffer concentration.

Next, the effect of glucose concentration is investigated. Figure 5 shows data for gold nanoparticle catalyst in 0.1 M phosphate buffer pH 7 for different glucose concentrations. At low glucose levels an approximately linear increase in glucose oxidation current is observed with plateauing at glucose concentration higher than 12 mM . This observation is in agreement with the Langmuirian binding model introduced above. The binding constant can be estimated (here from the point of third coverage, where

$$\Theta_G = \frac{K_G[G]}{1 + K_G[G] + K_P[P]} = \frac{1}{3} \text{ with } K_G[G] \approx K_P[P] \text{ as } K_G \approx 200 \text{ mol}^{-1} \text{ dm}^3.$$

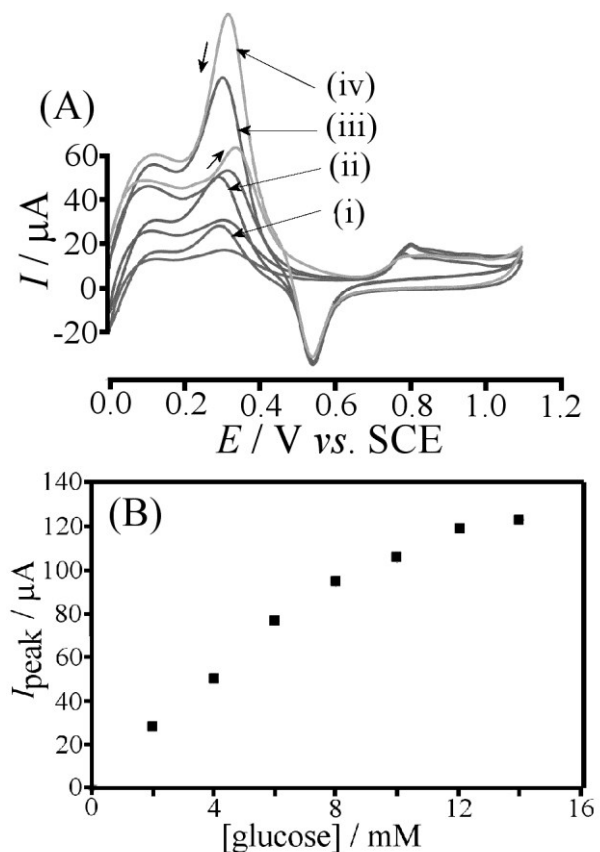


Figure 5. (A) Cyclic voltammograms (scan rate 5 mVs^{-1} , start point 0.0 V vs. SCE) for the oxidation of (i) 2, (ii) 4, (iii) 8, (iv) 14 mM glucose at gold nanoparticles on ITO immersed in 0.1 M phosphate buffer pH 7. (B) Plot of the peak current versus glucose concentration.

3.3. Suppressing Gold Nanoparticle Catalyst Poisoning with Polymer of Intrinsic Microporosity (PIM) Coating

Phosphate has been shown to compete with glucose for the active catalyst surface sites and many other molecules and ions potentially interfere or poison the catalyst surface. In

order to explore poisoning and the remediating effects of a porous PIM-EA-TB polymer film two cases are studied: (i) bovine serum albumin and (ii) chloride.

The coating of the polymer of intrinsic microporosity (PIM) PIM-EA-TB is applied by spin-coating to give approximately 500 nm thick films. This type of film has recently been shown to allow small ions and molecules such as formic acid to pass with electrocatalysts working just as well with or without this coating (demonstrated for formic acid oxidation on palladium [17]). Here the PIM coating is shown to not detrimentally affect the glucose oxidation (see Figure 6A) with clear oxidation peaks detected at 0.3 V vs. SCE. The plot of the peak current versus glucose concentration has an extended range into higher glucose concentrations (see Figure 6B). indicative of less competition to phosphate buffer (the activity of the phosphate buffer is believed to be lower in the PIM environment).

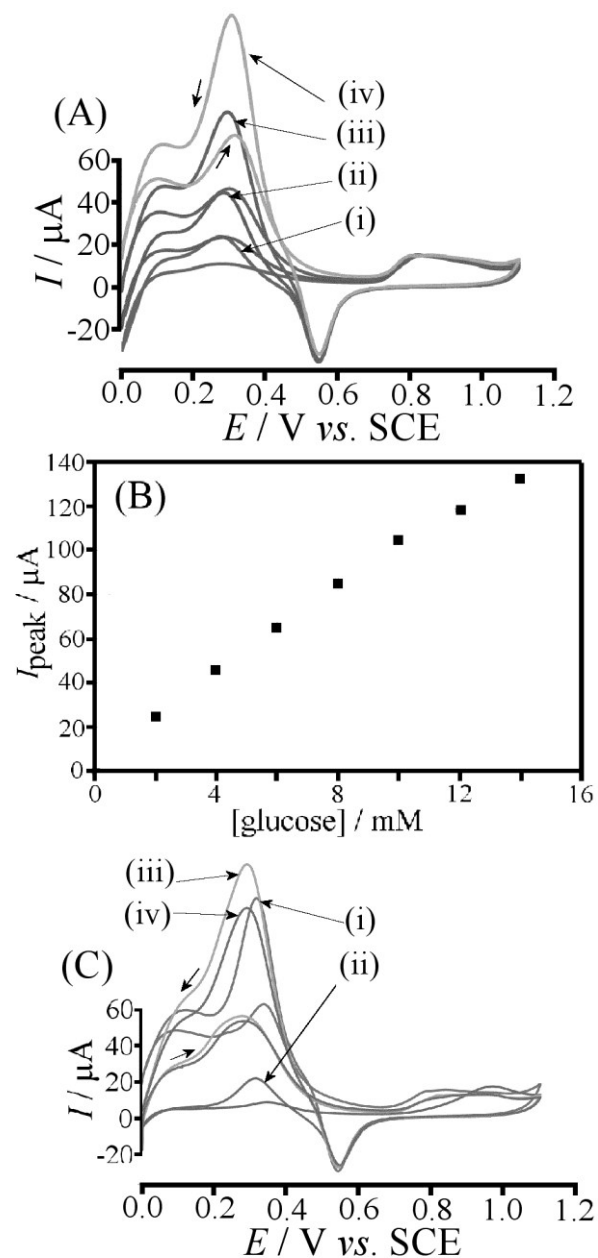


Figure 6. (A) Cyclic voltammograms (scan rate 5 mVs^{-1} , start point 0.0 V vs. SCE) for the oxidation of (i) 2, (ii) 4, (iii) 8, (iv) 14 mM glucose at gold nanoparticle on ITO, coated with 500 nm PIM, and immersed in 0.1 M phosphate buffer pH 7. (B) Plot of the peak current for glucose oxidation versus glucose concentration. (C) Cyclic voltammograms (scan rate 5 mVs^{-1}) for the oxidation of 14 mM glucose at gold nanoparticle on ITO immersed in 0.1 M phosphate buffer pH 7 (i) without and (ii) with BSA (3 mg in 50 cm^{-3} solution) and the same experiment with PIM coating (iii) without and (iv) with BSA.

When adding bovine serum albumin (BSA) as a known catalyst poison [29], a dramatic change is observed in the glucose oxidation current. Figure 6C (i) and (ii) show the current for glucose oxidation on bare gold nanoparticle catalyst before and after addition BSA (3 mg in 50 cm³ solution), respectively. The same experiment was repeated with PIM coating (see Figure 6C (iii) and (iv)) with no detrimental effect of the protein. It is likely that the PIM coating can repel the protein based on size exclusion.

A further severe poisoning effect on the gold nanoparticle electrocatalyst is induced by chloride. An addition of 10 mM chloride into 0.1 M phosphate buffer pH 7 almost completely eliminates the catalytic glucose oxidation (see Figure 7A (i) and (ii)). When the PIM coating is applied this effect is considerably less dramatic. In Figure 7A (iii) and (iv) the glucose oxidation for 8 mM glucose in 0.1 M phosphate buffer pH 7 is shown without and with 10 mM chloride, respectively, and only a 50% drop in current occurs. Therefore the PIM membrane changes the access of chloride to the catalyst surface (e.g. by competition of phosphate and chloride for PIM anion sites).

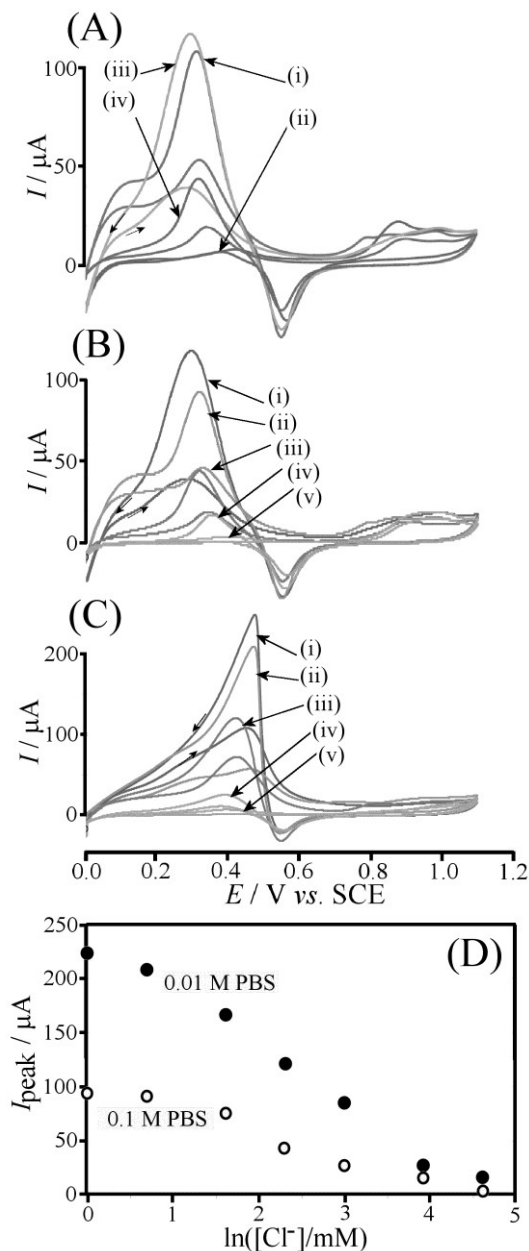


Figure 7. (A) Cyclic voltammograms (scan rate 5 mVs^{-1} , start point 0.0 V vs. SCE) for the oxidation of 8 mM glucose at gold nanoparticles on ITO immersed in 0.1 M phosphate buffer pH 7 (i) without and (ii) with 10 mM chloride and the same experiment with PIM coating (iii) without and (iv) with 10 mM chloride. (B) (A) Cyclic voltammograms (scan rate 5 mVs^{-1}) for the oxidation of 8 mM glucose at gold nanoparticles on ITO with PIM coating immersed in 0.1 M phosphate buffer pH 7 with (i) 0, (ii) 2, (iii) 10, (iv) 50, (v) 100 mM chloride. (C) (A) Cyclic voltammograms (scan rate 5 mVs^{-1}) for the oxidation of 8 mM glucose at gold nanoparticles on ITO with PIM coating immersed in 0.01 M phosphate buffer pH 7 with (i) 0, (ii) 2, (iii) 10, (iv) 50, (v) 100 mM chloride. (D) Plot of the peak current for glucose oxidation versus chloride concentration for 0.1 and 0.01 M phosphate buffer pH 7.

These experiments were repeated systematically for a range of chloride concentrations and for two phosphate buffer concentrations. The plot in Figure 7D shows both the effect of the lower buffer concentration increasing the glucose oxidation current and the effect of chloride reducing the catalyst activity. The observed data plot is again consistent with the model of competitive Langmuirian binding (equation 1). Interestingly, with the PIM coating the gold nanoparticle electrocatalyst is able to effectively operate even in 20 mM chloride. Typical blood serum levels of chloride are higher and therefore the improvement in catalyst performance is still not sufficient. However, the observed improvement with a thin PIM film coating is promising and future development could focus on (i) improved PIM materials in terms of molecular structure and pore structure for controlling access of poisons to the catalyst and (ii) improved design of the “electrocatalyst PIM environment” to optimise conditions in the reaction zone close to the active catalyst sites.

4. Conclusion

It has been shown that novel PIM materials such as PIM-EA-TB with extremely high surface area and ability to be protonated (to be semipermeable towards anions) provide a new class of electrochemically effective components for application in electrocatalysis, for example for energy harvesting and sensing. The rigid nature of the PIM polymer backbone minimises structural fluctuations and leads to a stable pore size for selective transport of neutral and charged species. When protonated, the PIM-EA-TB film exhibits

some degree of anion selectivity with potential benefits in electrocatalytic processes (e.g. widening the linear range, influencing competitive binding equilibria). Here, the oxidation of glucose on gold at pH 7 in phosphate buffer is investigated as a first model case. Three types of effects on the catalyst performance are observed:

- (i) The size selection effect of PIM pores allows poisoning from larger proteins such as bovine serum albumin to be suppressed
- (ii) The anion selection effect allows access of chloride to the catalyst surface to be reduced (in competition to phosphate)
- (iii) The change in anion activity in the catalyst reaction zone (e.g. reduced phosphate binding relative to glucose binding and extended linear range)

In future novel PIM materials could be designed and further improved by molecular control over pore size, pore shape, pore charge distribution, etc. In contrast to hydrogels, the novel PIM materials are highly stable and more dense to impose a stronger effect on the membrane permeability and catalyst environment. Rigidity and the molecular structure of the PIM polymer backbone play a key role in introducing new functionality and novel effects.

Acknowledgement

Y.R. thanks the University of Bath for a fee waiver.

References

-
- [1] A. Morozan, F. Jaouen, *Energy Environm. Sci.*, **2012**, 5, 9269.
- [2] Z. H. Dai, H. X. Ju, *TRAC-Trends Anal. Chem.*, **2012**, 39, 149.
- [3] A. Walcarius, *Chem. Soc. Rev.*, **2013**, 42, 4098.
- [4] D. M. Lin, J. F. Che, *Progress Chem.*, **2010**, 22, 1195.
- [5] T. F. Otero, J. G. Martinez, J. Arias-Pardilla, *Electrochim. Acta*, **2012**, 84, 112.
- [6] N. Ayres, *Polymer Chem.*, **2010**, 1, 769.
- [7] Z. H. Xiang, D. P. Cao, *J. Mater. Chem. A*, **2013**, 1, 2691.
- [8] P. M. Budd, B. S. Ghanem, S. Makhseed, N. B. McKeown, K. J. Msayib, C. E. Tattershall, *Chem. Commun.*, **2004**, 230.
- [9] N. B. McKeown, P. M. Budd, *Macromolecules*, **2010**, 43, 5163.
- [10] N. B. McKeown, B. Gahnem, K. J. Msayib, P. M. Budd, C. E. Tattershall, K. Mahmood, S. Tan, D. Book, H. W. Langmi, A. Walton, *Angew. Chem. Int. Ed.*, **2006**, 45, 1804.
- [11] S.V. Adymkanov, Y.P. Yampol'skii, A.M. Polyakov, P.M. Budd, K.J. Reynolds, N.B. McKeown, K.J. Msayib, *Polymer Sci.*, **2008**, 50, 444.
- [12] P. M. Budd, N. B. McKeown, B. S. Ghanem, K. J. Msayib, D. Fritsch, L. Starannikova, N. Belov, O. Sanfirova, Y. P. Yampol'skii, V. Shantarovich, *J. Membrane Sci.*, **2008**, 325, 851.
- [13] C. G. Bezzu, M. Carta, A. Tonkins, J.C. Jansen, P. Bernardo, F. Bazzarelli, N. B. McKeown, *Adv. Mater.*, **2012**, 24, 5930.

-
- [14] Y. Wang, N.B. McKeown, K.J. Msayib, G.A. Turnbull, I.D.W. Samuel, *Sensors*, **2011**, *11*, 2478.
- [15] D. Buenger, F. Topuz, J. Groll, *Progress Polymer Sci.*, **2012**, *37*, 1678.
- [16] A. Guiseppi-Elie, *Biomaterials*, **2010**, *31*, 2701.
- [17] F. J. Xia, M. Pan, S. C. Mu, R. Malpass-Evans, M. Carta, N. B. McKeown, G. A. Attard, A. Brew, D. J. Morgan, F. Marken, *Electrochim. Acta*, 2013, in press.
- [18] M. Carta, R. Malpass-Evans, M. Croad, Y. Rogan, J. C. Jansen, P. Bernardo, F. Bazzarelli, N. B. McKeown, *Science*, **2013**, *339*, 303.
- [19] M. Arredondo, M. Stoytcheva, R. Zlatev, V. Gochev, *Mini-Rev. Medicinal Chem.*, **2012**, *12*, 1301.
- [20] G. F. Wang, X. P. He, L. L. Wang, A. X. Gu, Y. Huang, B. Fang, B. Y. Geng, X. J. Zhang, *Microchim. Acta*, **2013**, *180*, 161.
- [21] Q. Liu, X. H. Xu, G. L. Ren, W. Wang, *Progress Chem.*, **2006**, *18*, 1530.
- [22] Y. Li, Y. Y. Song, C. Yang, X. H. Xia, *Electrochem. Commun.*, **2007**, *9*, 981.
- [23] Y. G. Zhou, S. Yang, Q. Y. Qian, X. H. Xia, *Electrochem. Commun.*, **2009**, *11*, 216.
- [24] M. Pasta, F. La Mantia, Y. Cui, *Electrochem. Commun.*, **2010**, *12*, 1407.
- [25] L. Rassaei, F. Marken, *Anal. Chem.*, **2010**, *82*, 7063.
- [26] A. Martins, V. Ferreira, A. Queirós, I. Aroso, F. Silva, J. Feliu, *Electrochem. Commun.*, **2003**, *5*, 741.
- [27] A. Celebanska, A. Lesniewski, M. Paszewski, M. Jonsson-Niedziolka, J. Niedziolka-Jonsson, M. Opallo, *Electrochem. Commun.*, **2011**, *13*, 1170.
- [28] H. du Toit, M. Di Lorenzo, *Sens. Actuators B-Chem.*, **2014**, *192*, 725.

-
- [29] Y. Chen, K. Flowers, M. Calizo, S.W. Bishnoi, *Coll. Surfaces B-Biointerfaces*, **2010**, 76, 241.